Multi-objective parametric optimization of driver-based electromagnetic sheet metal forming of SS304 using AA6061-T6 driver.

KHAN, Z., KHAN, M., YOUNAS, M., DANISH, A.S., KHAN, A. and DJAVANROODI, F.

2024

Optimizing Process Parameters using Multi-Objective Techniques for Driver-Based Electromagnetic Forming of SS304 and AA6061-T6 driver.

Zarak Khan[a], Mushtaq Khan[b], Muhammad Younas[c], Abdul Samad Danish[d], Ashfaq Khan[c], andFaramarz Djavanroodi[b]

aDepartment of Mechanical Engineering, HITEC University, Taxila, Pakistan;

bMechanical Engineering Department, Prince Mohammad BinFahd University, Al-Khobar, Saudi Arabia;

cSchool of Engineering, Robert Gordon University, Aberdeen, UK;

dDepartment of ComputerScience, HITEC University, Taxila, Pakistan

Abstract

This study uses statistical techniques to optimize the electromagnetic forming process for driver-based sheet metal forming with a flat coil. AA6061T6 sheet was used as a driver to form SS304sheets. The optimization of maximum elongation, die fitting, maximum Lorentz force, and peakcurrent was carried out. The results were verified through simulation which were in close agree-ment with the experimental results. The most influential factor was the voltage (C.R of 72.97%),followed by coil gap and SS304 sheet thickness (7.99 and 6.07%, respectively).

1 Introduction

Lightweight metals are in very high demand in the automobile, aerospace, and process industries. The major share of lightweight manufacturing is captured by aluminum alloys because of their better strength-to-weight ratio. Recently high-speed electromagnetic forming of Aluminum and Magnesium is substituting conventional forming processes because of its added advantages most important of which is better formability [1], [2] [3]. The performance of an electromagnetic forming process depends upon the process parameters such as electrical energy, actuator coil geometry, the gap between the workpiece and coil [4]. The effect of coil geometry and its numerical validation was carried out by [5]. A concave coil was used to enhance the electromagnetic forming of AA6063-T6 tube. The concave coil with suitable process parameters resulted in more homogenized deformation compared to the simple cylindrical coil. An arrangement of three coils was used by [6] to enhance the formability of the aluminum tube by introducing additional axial forces along with the radial magnetic force. The depth of deformation was enhanced at the expense of sheet thickness reduction. The electromagnetic forming process was analyzed by [7], with a focus on the effects of various parameters such as initial charging voltage, workpiece material, geometry, and holding devices. Both theoretical analysis and FE modeling are used to study the process, with the Lorentz force acting on the workpiece as the primary dependent variable. Numerical and analytical results show good agreement, providing practical insight into the process and improving our understanding of its principles. [8] analyzed the variation of inductance and resistance of the coil due to changes in these parameters and establishes their effect on the current pulse and deformation of a tube. Q-factor of the coil is also analyzed to determine its losses. Experimental and numerical validation was performed by deforming an aluminum AA 6061 tube. Small changes in diameter and number of turns can significantly impact the amplitude of the current pulse, and the addition of a parallel discharge cable can improve current and

frequency. [9] explored the feasibility of an inexpensive electromagnetic forming (EMF) process for fast manufacturing of 3-D microstructures on the inside well of a wound thin tube. The process involved winding a copper film onto a forming mandrel and inserting it into a forming coil that applied external compressive force using the EMF process. A cost-effective method was proposed for manufacturing the forming mandrel using reverse electro-discharge machining. The study investigated the effects of tube thickness and proposed a composite tube to improve forming depth and profile completeness of the microstructure. 3D finite element analysis toolbox for Electromagnetic forming (EMF) was developed by [10] using the FORGE software and had acquired an EMF machine to study material behavior at high deformation speeds. The study describes the modelling strategy and presents results for a ring expansion case, as well as experimental settings and preliminary results for direct free forming of flat metal sheet. The electromagnetic compression of AA6061 tubes using finite element method simulation and experimental analysis was investigated by [11]. The effect of energy generated from single and/or double capacitor banks and the gap between the coil inner diameter and tube OD on deformation was analyzed. Numerical calculations of velocity, magnetic field, effective plastic strain, displacement, and current density were compared, and a regression equation was developed to calculate rib depth. A correlation between discharge energy and gap with tube deformation was established, and the variation of numerically calculated parameters was analyzed.A dual coil configuration was used by [12] to increase the deformation depth of the aluminum sheet by introducing axial magnetic force along with radial magnetic force. The electromagnetic attractive force was created using two discharge circuits by [13] to deform a small tube configuration where coils cannot be placed inside the tube. Driver-based sheet metal stamping of steel was carried out by [14] using aluminum as a driver, the results showed enhanced formability of stamped steel sheets compared to quasistatic stamping.

The effect of aluminum driver sheet thickness on the deformation height of DP780 steel workpiece was studied by [15]. The thicker sheet resulted in a better deformation of the steel workpiece. Similar work was carried out by [16] in which the Ti-6Al-4V alloy sheet was deformed using copper and aluminum sheets as a driver. The deformation of the workpiece improved by using a thick driver sheet of aluminum alloy as compared to the thin sheet while in copper alloy driver the trend was reversed because the deformation of the driven sheet is not only dependent upon the electrical conductivity of the driver sheet but also on its strength. A numerical simulation was carried out by [17] to estimate the deformation of titanium alloy using aluminum alloy as a driver. The electromagnetic forces were estimated using ANSYS/EMAG the results of which were then transferred to ABAQUS using subroutine code. The process was suggested to be very accurate for stamping and embossing the workpiece.

A new type of tube with varying thickness and lateral corrugation was developed and optimized for energy absorption by [18]. Two versions with different corrugation numbers were analyzed and the one with 6 corrugations was found to be more scalable. The optimized design showed a significant improvement in energy absorption and reduction in maximum force compared to the original design. To optimize the process parameters of electromagnetic tube forming an algorithm was developed by [19] for specified bead depth. The die entrance radius, input energy, and tube thickness were the main process-controlling parameters. Taguchi design of experiments and ANOVA was used by [20] to analyze the effects of input energy, the number of coil turns and sheet thickness on the final deformation height of the closed die AA6061-T6 sheet. The input energy and sheet thickness have a significant effect on the final deformation. The hybrid joining process of Cu-SS tubes using electromagnetic forming and adhesive was investigated by[21] and important parameters with their contribution to pull out and compressive strength of the joint were identified using ANOVA. In a similar work, an electromagnetic welding process was investigated using the response surface method (RSM) by [22] to find the effect of input energy, standoff distance, and distance between the spacers on the ultimate tensile strength and hardness of the weld. RSM

was used to optimize the process parameters of electromagnetic welding of Al-Cu by [23]. Two-stage electromagnetic forming of perforated aluminum sheets was carried out and optimized deformation force was estimated using RSM and ANOVA [24]. The effect of workpiece thickness, input voltage, and workpiece and coil clearance on the Electromagnetic tube compression process was investigated [25]. Johnson Cook's damage model was used to estimate the tearing of the workpiece material. A regression equation was developed by [11] to investigate the process parameters of electromagnetic compression. The major contributing parameter was the electrical energy supplied. Another investigation on process parameters optimization of electromagnetic free bulging was performed by [26]. The optimized results were validated through experiments. Driver-based electromagnetic forming of Al metal using copper as a driver was carried out by [27]. It was observed that the forming height increased with the addition of a copper driver plate as compared to the simple forming of Al without the driver.

In this research, the focus is on four important process parameters of a driver based closed die electromagnetic forming namely thickness of AA6061-T6 driver sheet, SS304 driven sheet thickness, input voltage, and standoff distance between the workpiece and tool coil. The responses measured and estimated were maximum sheet elongation (SS304), Die fitting, maximum magnetic pressure, and peak current. Taguchi design of experiments was used to produce L9 array (L9 3^4) for ANOVA and multi-objective optimization of the electromagnetic forming process.

2 Experimental setup and Forming responses.

In this study, SS304 steel was employed as the material for the workpiece. The AA6061-T6 alloy was utilized as the driver to transmit the magnetic force from the coil to the non-magnetic workpiece. Experiments were conducted utilizing a closed die made of Austenitic Steel that had a central block. The experimental configuration comprised of a tool coil that was secured within a fiber wood frame using epoxy. It was connected to a capacitor bank (6×10^{-3} F) through high ampere wires and powered by a power supply that varied between 200 V to 3000 V. The setup had a system inductance of 3.63×10^{-6} and resistance of 0.02 Ω. A diagram of the experimental setup can be seen in Figure 1. The electromagnetic forming conditions along with the levels are tabulated in table 1. The levels of process parameters were selected based on previous literature and the capability of the available electroforming machine [20], [28]. The response parameters include the maximum elongation of SS304 after deformation (R1), the distance between forming die and the workpiece after deformation also known as die fitting (R2), the maximum magnetic force (R3), and peak current (R4). For measuring the minimum sheet thickness the location was identified using a numerical model as shown in Figure 2. The thickness was measured twice using a vernier gauge for each experimental condition. The die fitting was also measured using the technique discussed in the previous research [20], [28]. The magnetic force was estimated by using the validated fully-coupled numerical model developed in COMSOL Multiphysics [28], [29] as shown in Figure 3. The peak current values were measured both experimentally by a Rogowski coil and numerically. The numerical and experimental current plot is shown in Figure 4. Figure 5 represents the deformed SS304 work piece.

Figure 1 Electromagnetic forming machine

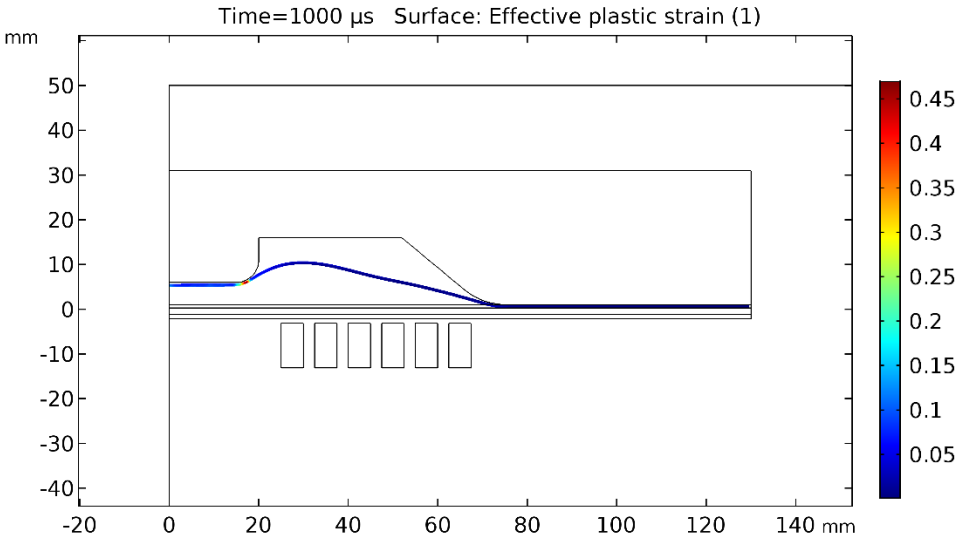

Figure 2

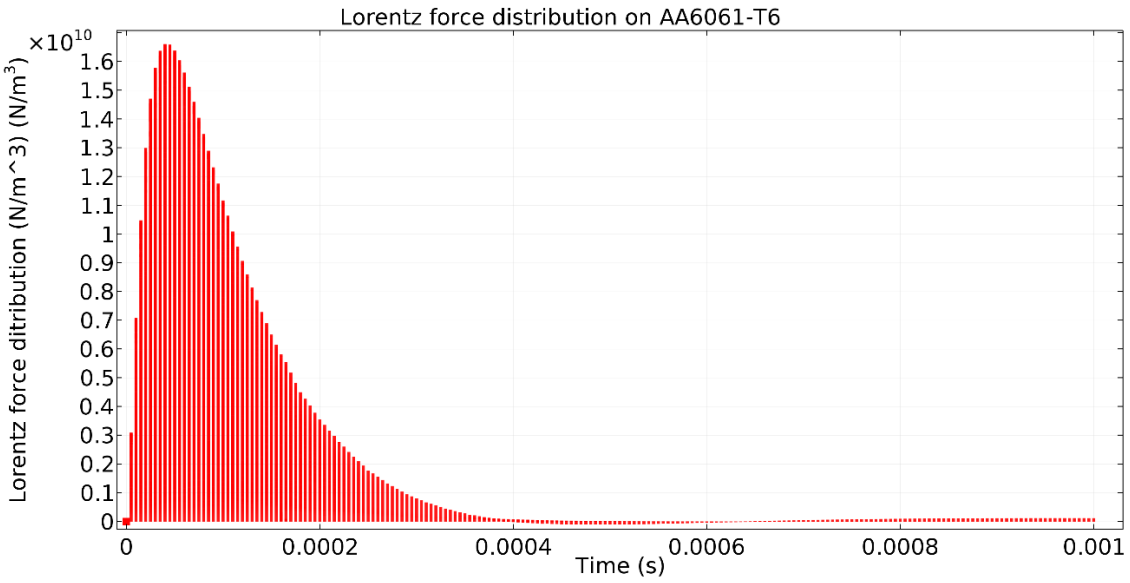

Figure 3

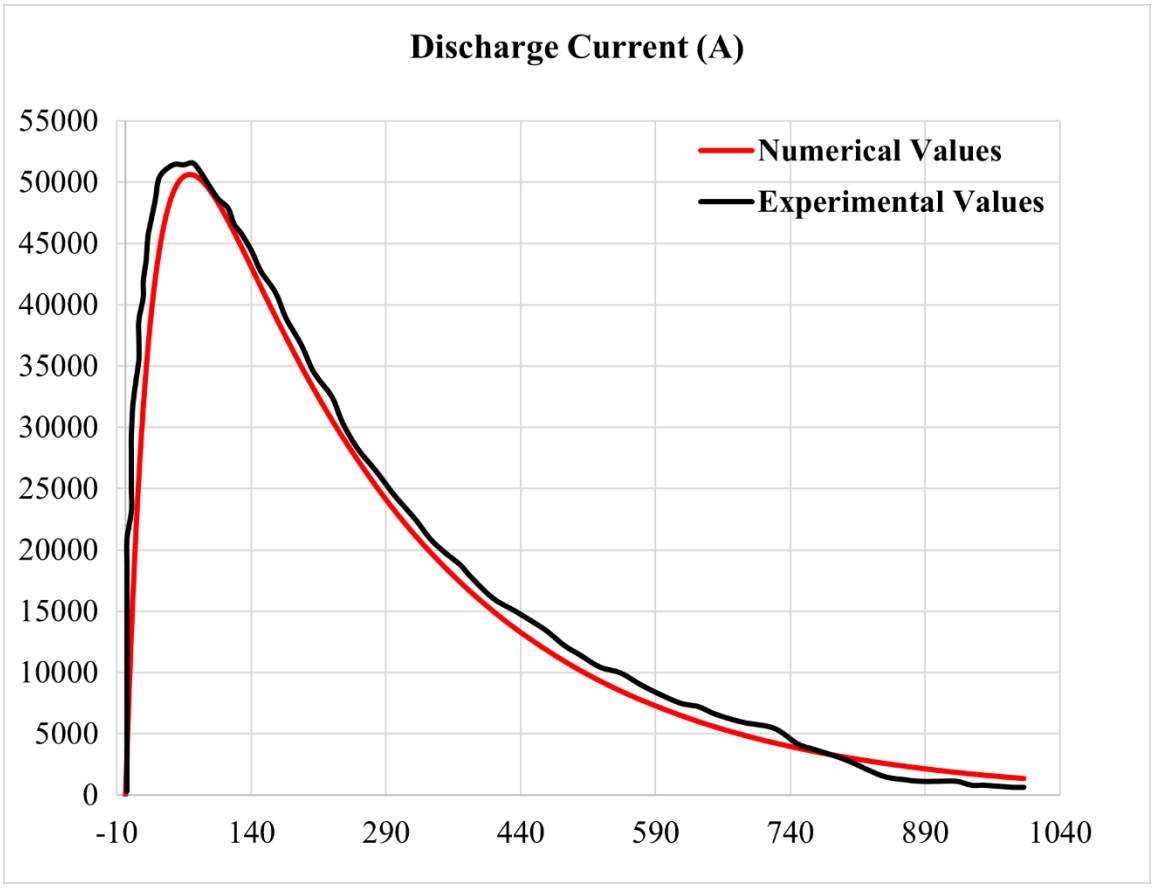

Figure 4

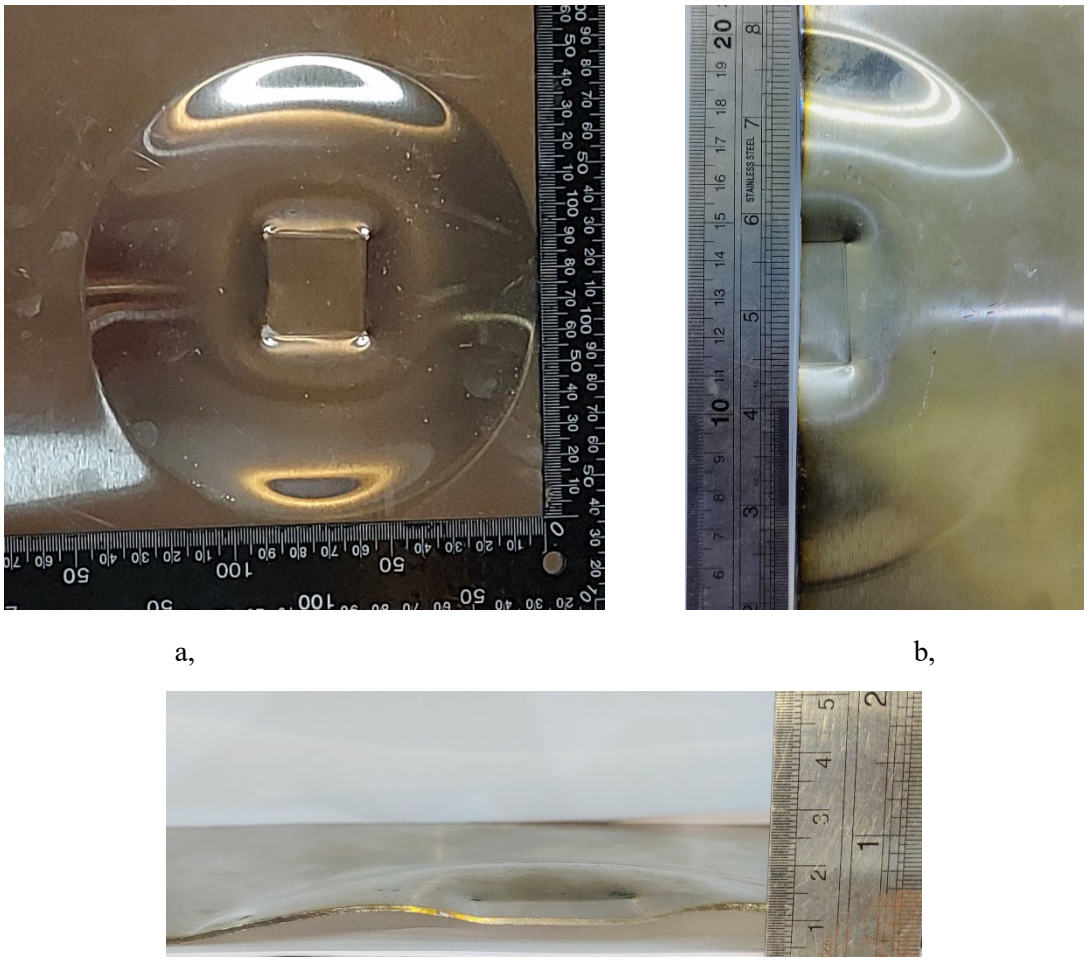

a, b,

c

Figure 5 SS304 workpiece from various views a, Top view b, Half section top view c, Front view

Table 1 Forming process parameters with their levels

Process Parameters		Level 1	Level 2	Level 3
SS304 thickness (mm)	(P1)	0.56	0.71	1.02
AA6061-T6 Thickness (mm)	(P2)	1.16	1.42	2
Input Voltage (V)	(P3)	2400	2600	2800
Coil/Workpiece standoff distance (mm)	(P4)	1	2	3

2.1 Design of experiment

In table 2, a Taguchi L9 array with 3^4 elements was generated through Minitab software. The responses were obtained by conducting two measurements and averaging the results to decrease any inaccuracies. The main effect plots were used to individually analyze the responses, while the Response Surface Methodology (RSM) was utilized to examine multiple responses. A weighting method based on equality was applied, and a regression model was established using the Grey relation. Finally, the outcomes from the statistical analysis were experimentally confirmed.

Table 2 Experiments using the L9 array and their responses.

Exp #	SS304 Thickness (P1) (mm)	AA6061-T6 Thickness (P2) (mm)	Voltage (P3) (V)	Coil Gap (P4) (mm)	Maximum Elongation (R1) (mm/mm)	Die fitting (Δx) (R2) (mm)	Max Magnetic pressure (R3) x10^10(N/m^3)	Peak current (R4) (A)
1	0.56	1.16	2400	1	0.344	4.95	1.34	43200
2	0.56	1.42	2600	2	0.433	4.99	1.26	46800
3	0.56	2	2800	3	0.530	5.74	1.21	50300
4	0.71	1.16	2600	3	0.280	5.9	1.245	46400
5	0.71	1.42	2800	1	0.430	4.2	1.66	50700
6	0.71	2	2400	2	0.226	7.35	1.015	43300
7	1.02	1.16	2800	2	0.250	6	1.61	50200
8	1.02	1.42	2400	3	0.150	8.1	0.95	42900
9	1.02	2	2600	1	0.220	7.15	1.37	47000

2.2 Experimental data analysis

The measured data obtained from all the response parameters (R1, R2, R3, R4) was assessed to analyze the effect of forming process parameters (P1, P2, P3, P4) on these responses. Figure 6 presents the trend of all response parameters independently of each process parameter in the main effect plot. The trend for maximum elongation of the workpiece sheet (SS304) is presented in Figure 6a. The elongation of SS304 decreases with an increase in the thickness of the driven SS304 sheet. Although with the increase in sheet thickness the magnetic force due to lower magnetic flux losses increases but this increase is much lower than the increase in mechanical strength of the workpiece for thicker sheets [30]. The AA6061-T6 driver sheet thickness results in better elongation of SS304 at 1.42 mm compared to 1.16mm and 2mm. By increasing the voltage, the elongation of the workpiece increases this is because of the increase in magnetic force. The maximum elongation results in a minimum standoff distance between the coil and the driver sheet.

The die fitting is related to the deformation of the workpiece, greater deformation will result in better die fitting and hence a smaller value of Δx [20]. From figure 6b the smaller the better is applied, it can be observed that the die fitting Δx decreases by decreasing the sheet thickness of the driver as well as the driven sheet in the given ranges of the process parameters. By increasing the voltage and decreasing the stand-off distance between the coil and driver sheet the die fitting will decrease which is favorable.

The magnetic pressure increases with the increase in voltage because of higher electrical energy and decreases with the increase in the stand-off distance between the coil and the driver sheet. SS304 workpieces do not have much impact on magnetic force as evident from figure 6c. The peak current is highest at higher voltage and lowest at lower voltage because of the increase in induced current at higher voltage as shown in figure 6d. By reducing the stand-off distance between the coil and the workpiece the peak current increases.

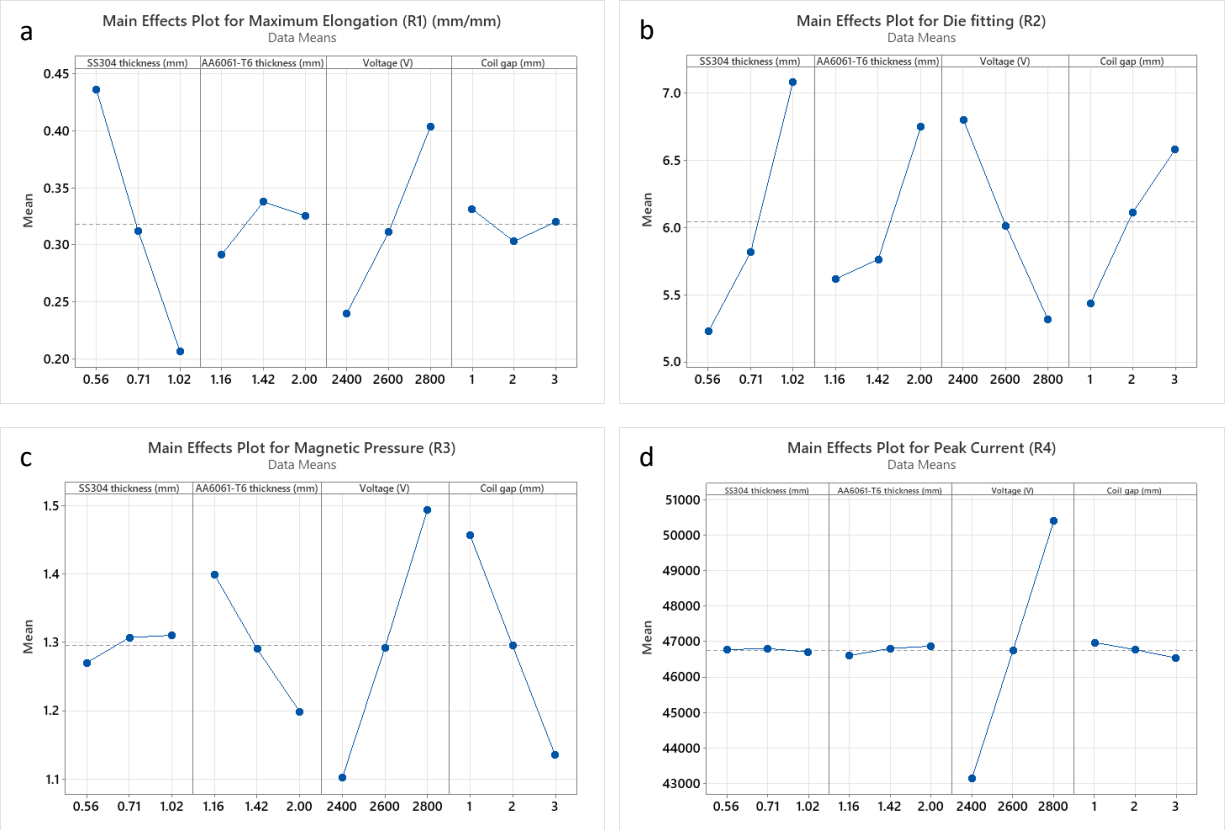

Figure 6 Main effect plots of response parameters (a) Maximum elongation of SS304, (b) Die fitting, (c) Maximum magnetic pressure, (d) Peak current

Table 3 Electromagnetic forming combinations for individual best and worst response

Input parameters	**Responses**							
	Elongation (R1) (mm/mm)		Die fitting (R2) (mm)		Magnetic pressure (R3) x10^10(N/m^3)		Peak Current (R4) (A)	
	Best	Worst	Best	Worst	Best	Worst	Best	Worst
SS304 thickness (mm)	0.56	1.02	0.56	1.02	1.02	0.56	0.56	1.02
AA6061-T6 thickness (mm)	1.42	1.16	1.16	2.00	1.16	2	2	1.16
Voltage (V)	2800	2400	2800	2400	2800	2400	2800	2400
Coil gap (mm)	1	2	1	3	1	3	1	3

2.3 Grey relation analysis for multi objective optimization

In the electromagnetic forming process improvement one all response parameters are not possible, instead, there is always a trade-off. Improvement of one response may result in the lessening of other responses. To solve this issue the method of multi objective optimization is very useful. The technique used in this research is adopted from the work of [31][32], the flow chart of the optimization method is given in figure 7. Grey relation analysis was performed (GRA), and equal weightage was given to all response parameters therefore analytical hierarchy process was not required. All the steps involved in the optimization process are as follows.

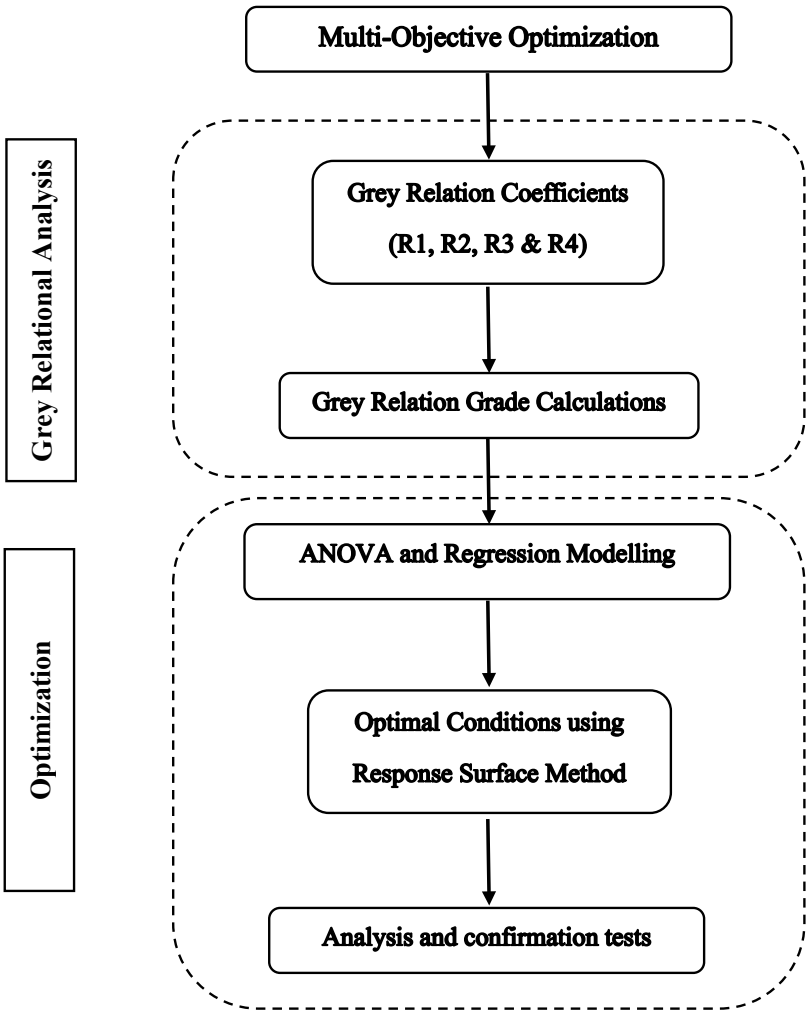

Figure 7 Multi-Objective Optimization methodology

3 Data processing

To begin with Grey relation analysis all the responses were normalized by converting them to a common scale ranging from 0-1 [33]. The objective of normalization varies for different responses. Response like maximum elongation (R1), max magnetic pressure (R3), and peak current (R4) are to be maximized while the die fitting (Δx) (R2) is to be minimized in this research work. The "larger the better" approach was used

for the normalization of R1, R3, and R4 using Eq. 1, and for R2 the "smaller the better" approach was followed using Eq. 2.

$$Z_{ij} = \frac{y_{ij} - \min\,(y_{ij}, i = 1, 2, \ldots . n)}{\max\left(y_{ij}, i = 1, 2, \ldots . n\right) - \min\,(y_{ij}, i = 1, 2, \ldots . n)} \qquad (1)$$

$$Z_{ij} =< \frac{\max\left(y_{ij}, i = 1, 2, \ldots . n\right) - y_{ij}}{\max\left(y_{ij}, i = 1, 2, \ldots . n\right) - \min\,(y_{ij}, i = 1, 2, \ldots . n)} \qquad (2)$$

Where max (y_{ij}) and min (y_{ij}) represent the maximum and minimum values of respective responses furthermore Y_{ij} and Z_{ij} represent the actual and normalized values respectively.

4 Calculation of grey relation coefficient

The grey relation coefficients (GRC) for each response are calculated using the normalized values and Eq. 3.

$$\gamma\,(Z_o\,, Z_{ij}) = \frac{\Delta\min + \xi\Delta\max}{\Delta oj(k) + \xi\Delta\max} \qquad (3)$$

$$0 < \gamma\,(Z_o\,, Z_{ij}) \leq 1$$

The maximum and minimum value of the deviation sequence is represented by Δmax and Δmin respectively. Eq. 4 represents the relation for calculating the deviation sequence Δoj(k).

$$\Delta oj(k) = \left|Z_o(k) - Z_{ij}(k)\right| \qquad (4)$$

Where Z_0(k) and Z_{ij} (k) denote the reference sequence and comparability of each response respectively. In the current research, the value of the distinguishing factor (ξ) is kept at 0.5 to assign all the parameters equal weightage. The GRC values for all response parameters (R1, R2, R3, and R4) are tabulated in table 4.

Table 4 Calculated values of GRC and GRG from the responses

Exp	SS304 Thickness (mm)	AA6061-T6 Thickness (mm)	Voltage (V)	Coil Gap (mm)	GRC	GRC	GRC	GRC	GRG
	P1	P2	P3	P4	R1	R2	R3	R4	
1	0.56	1.16	2400	1	0.5053	0.7222	0.5259	0.3421	0.5239
2	0.56	1.42	2600	2	0.6620	0.7117	0.4702	0.5000	0.5860
3	0.56	2	2800	3	1.0000	0.5587	0.4410	0.9070	0.7267
4	0.71	1.16	2600	3	0.4318	0.5342	0.4610	0.4756	0.4757
5	**0.71**	**1.42**	**2800**	**1**	0.6552	1.0000	1.0000	1.0000	**0.9138**
6	0.71	2	2400	2	0.3846	0.3824	0.3550	0.3451	0.3668
7	1.02	1.16	2800	2	0.4043	0.5200	0.8765	0.8864	0.6718
8	1.02	1.42	2400	3	0.3333	0.3333	0.3333	0.3333	0.3333
9	1.02	2	2600	1	0.3800	0.3980	0.5504	0.5132	0.4604

5 Calculation of GRG

The multiple GRC obtained are converted into a combined factor called grey relational grade (GRG). In the present research equal, weights were assigned to all GRCs [34]. Optimum results can be obtained by maximizing the GRG value. Eq. 5 and Eq. 6 are used to calculate the GRG and the weightage respectively.

$$\text{Grade}\left(Z_0, Z_{ij}\right) = \sum_{k=1}^{n} \omega_k \, \gamma\left(Z_o\,, Z_{ij}\right) \qquad (5)$$

$$\sum_{k=1}^{n} \omega_k = 1 \qquad (6)$$

6 Result and discussion

After ranking the GRG values the best result out of all experimental conditions was observed for experiment number 5 corresponding to parameters (SS304 = 0.71 mm, AA6061-T6 = 1.41 mm, voltage = 2800 V, Coil gap = 1 mm) as shown in table 4.

6.1 Regression model for GRG function

A second order model of RSM was used to develop a multi-objective function of GRG. The insignificant terms were removed from the equation. The predicted GRG was obtained by using regression relation (Eq. 7). The predicted values matched well with the experimental results with the maximum error of 2% as shown in figure 8.

*GRG= -5.974 + 6.678 SS304 Thickness + 0.718 AA6061-T6 Thickness + 0.002324 Voltage - 0.1508 Coil Gap - 1.008 SS304 Thickness*AA6061-T6 Thickness - 0.002061 SS304 Thickness*Voltage (7)*

The GRG model is limited to the electromagnetic forming of SS304 with AA6061-T6 driver sheet within the conditions and ranges mentioned in table 1.

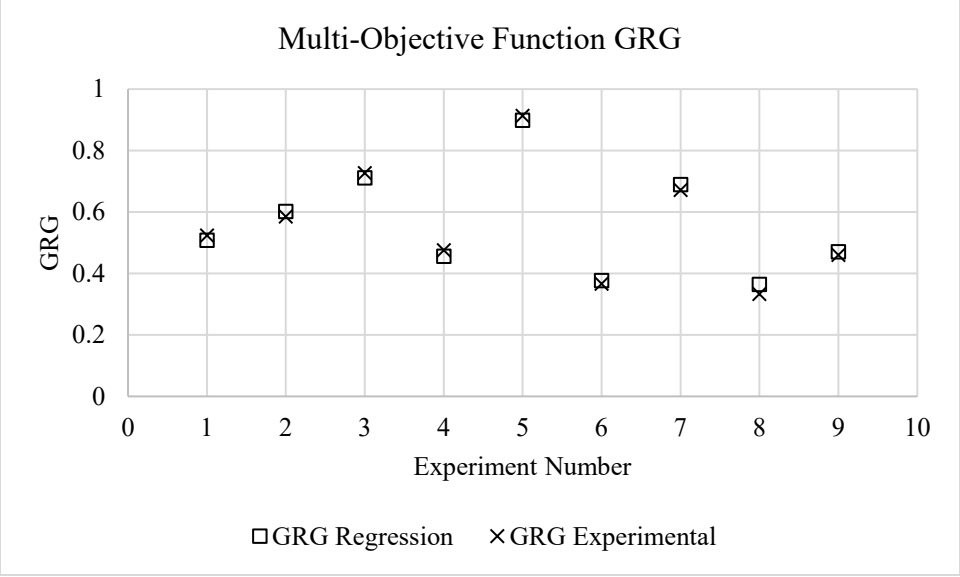

Figure 8 GRG obtained experimentally and calculated from the regression model

Contour and surface plots of GRG for electromagnetic forming conditions under study are shown in figure 9 and figure 10. The surface plots represent the effects of electromagnetic forming parameters on the obtained GRG. In figure 10 only the surface plot of SS304 thickness and Voltage vs GRG and Coil gap and Voltage vs GRG were plotted because the contribution ratios of Voltage, SS304 sheet thickness and Coil gap were the highest as evident from table 9. From figure 6a the maximum value of GRG was observed at lowest value of SS304 sheet thickness and highest value of the voltage. Furthermore, figure 10b reveals that the observed GRG was maximum at lowest value of Coil gap and highest value of Voltage.

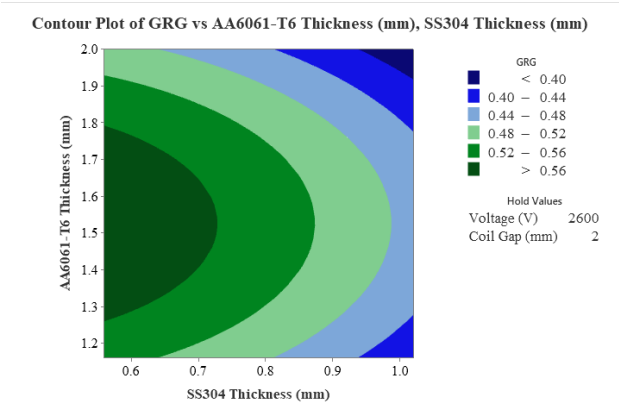

(a)

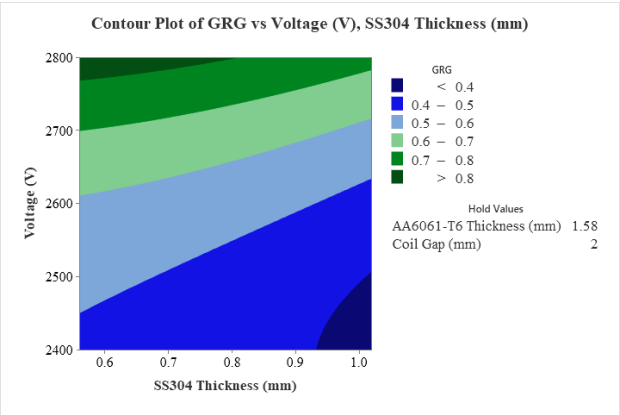

(b)

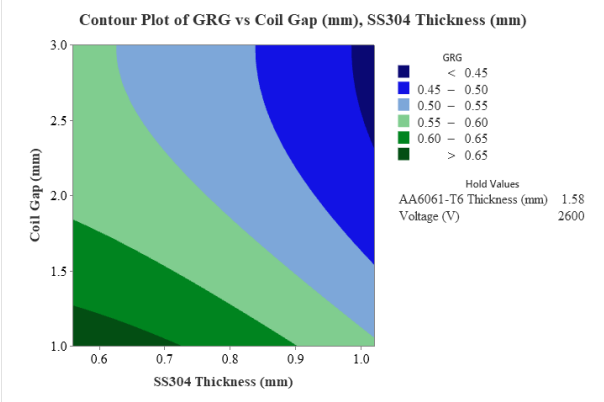

(c)

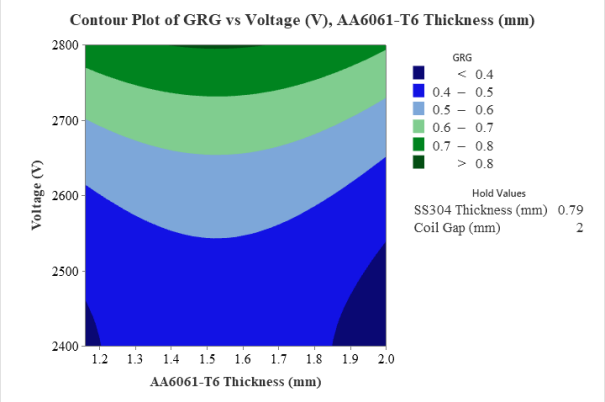

(d)

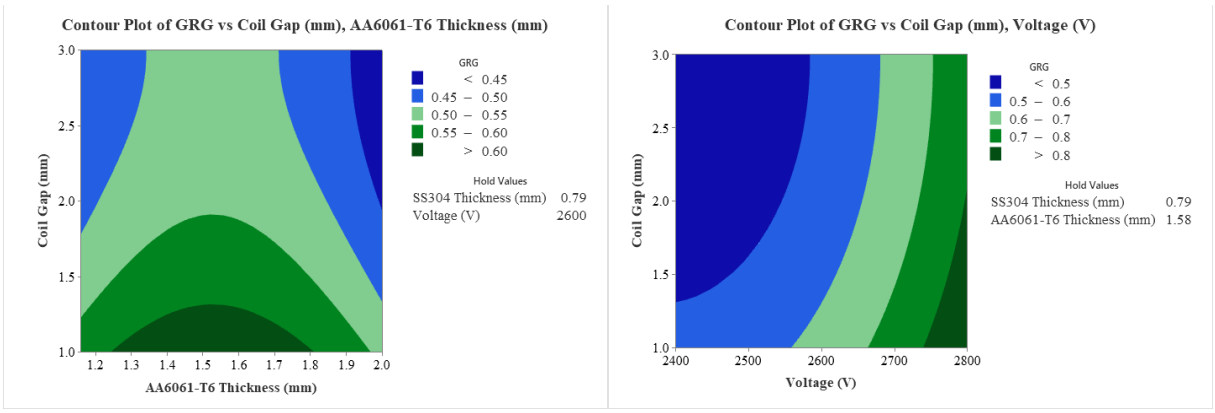

(e) **(f)**

Figure 9 Contour plots of GRG for electromagnetic forming. GRG vs ((a) AA6061-T6 and SS304, (b) Voltage and SS304, (c) Coil gap and SS304, (d) Voltage and AA6061-T6, (e) Coil gap and AA6061-T6, (f) Coil gap and Voltage)

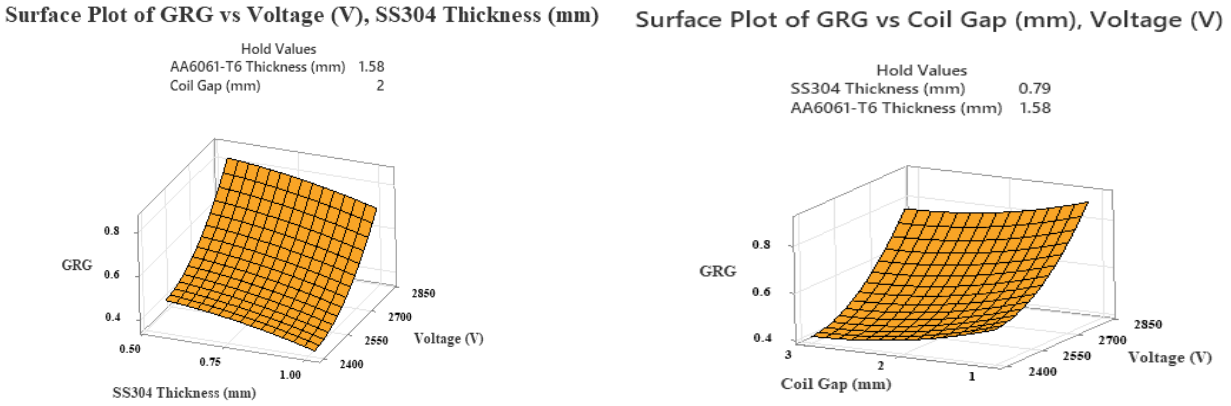

(a) **(b)**

Figure 10 Surface plots of GRG for Electromagnetic forming process (a) GRG vs Voltage (V) and SS304 sheet thickness (mm) (b) GRG vs Coil gap (mm) and Voltage (V)

6.2 ANOVA for GRG

A statistical analysis was performed using MINITAB software to examine the effect of electromagnetic forming parameters (SS304 thickness, AA606-T6 thickness, voltage, and coil gap) on sheet metal forming responses and GRG. ANOVA was conducted at a 95% confidence level. The results indicated that a quadratic model provided the best fit, with an R2 value of 98%. The analysis of variance revealed that the interaction between SS304 thickness (mm) and voltage (V) was a significant factor in affecting sheet metal forming responses and GRG. However, among the individual parameters, voltage was the most influential, with a contribution ratio of 72.97%. Coil gap and SS304 thickness were the next most important factors, with contribution ratios of 7.99% and 6.07%, respectively. The interaction between SS304 thickness and

voltage had a contribution ratio of 7.02%. AA606-T6 thickness and its interactions with other parameters had the least influence.

Table 5 ANOVA of GRG

Source	DF	Seq SS	Contribution	Adj SS	Adj MS	F-Value	P-Value
Regression	7	0.49736	98.92%	0.49736	0.07105	130.85	0
SS304 Thickness (mm)	1	0.03054	6.07%	0.04012	0.04012	73.9	0
AA6061-T6 Thickness (mm)	1	0.00791	1.57%	0.00283	0.00283	5.21	0.046
Voltage (V)	1	0.36690	72.97%	0.02449	0.02449	45.12	0
Coil Gap (mm)	1	0.04018	7.99%	0.08915	0.08915	164.19	0
SS304 Thickness (mm)*AA6061-T6 Thickness (mm)	1	0.01647	3.28%	0.02998	0.02998	55.22	0
SS304 Thickness (mm)*Voltage (V)	1	0.03530	7.02%	0.03010	0.03010	55.44	0
AA6061-T6 Thickness (mm)*Voltage (V)	1	0.00003	0.01%	0.00003	0.00003	0.07	0.804
Error	10	0.00543	1.08%	0.00543	0.00054		
Lack-of-Fit	1	0.00173	0.34%	0.00173	0.00173	4.21	0.07
Pure Error	9	0.0037	0.74%	0.0037	0.00041		
Total	17	0.50279	100.00%				

6.3 Optimization of response surface model for GRG

The response surface optimization process was used to find the best electromagnetic sheet metal forming conditions for the model developed in Eq. (7). The optimized results in Fig. 11 shows the maximum GRG value obtained at the highest level of the electromagnetic forming settings (SS304 thickness= 0.56 mm, AA6061-T6 thickness = 1.52 mm, Voltage = 2800 V and Coil gap = 1 mm).

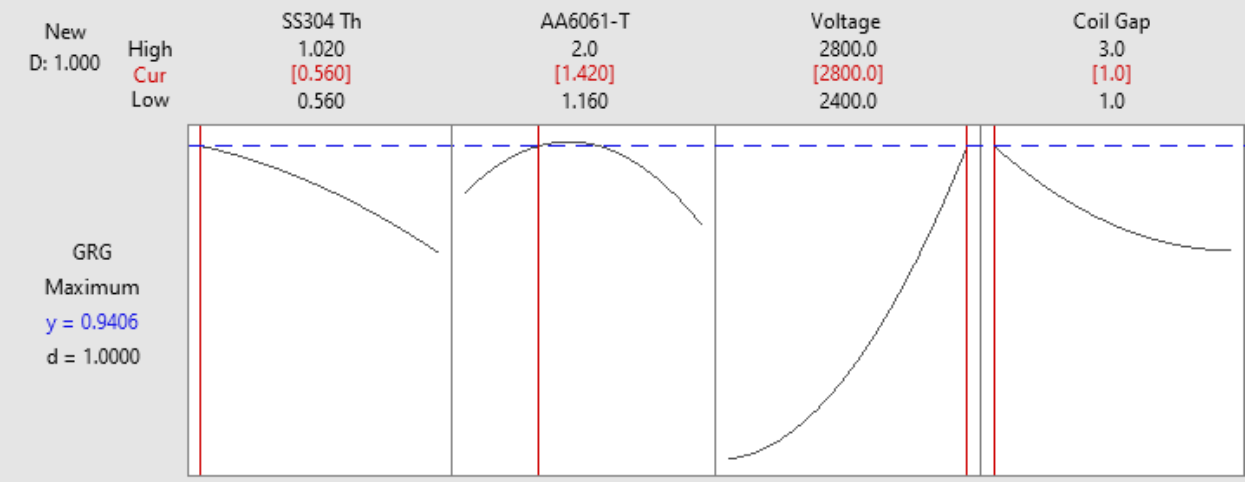

Figure 11 Response optimized at maximum GRG

6.4 Validation experiments

Table 6 presents the comparison of best experimental run (Exp # 5) from L9 array with optimized electromagnetic forming parameters obtained from response surface. The results obtained indicates considerable improvement in elongation and die fitting responses by 28.3 % and 29% respectively while small increase was observed in magnetic pressure (0.6%) and peak current (0.2%).

The comparison of the parameters used in best experimental run and optimized parameters identifies the most important parameter as SS304 sheet thickness on the other hand AA6061-T6, Voltage and Coil gap have the same values.

Table 6 Comparison of best experimental parameters with optimized parameters

Exp #	SS304 (P1) (mm)	AA6061 -T6 (P2) (mm)	Voltage (P3) (V)	Coil Gap (P4) (mm)	Maximum Elongation (R1) (mm/mm)	Die fitting (Δx) (R2) (mm)	Max Magnetic pressure (R3) x10^10 (N/m^3)	Peak current (R4) (A)
Best Run	0.71	1.42	2800	1	0.430	4.2	1.66	50700
Optimized run	0.56	1.42	2800	1	0.6	3.25	1.67	50600
% Change					28.3%	29%	0.6%	0.2%

7 Conclusion

In this study the optimal parameters were achieved using multi-objective optimization of electromagnetic forming responses to gain the sustainable goal of manufacturing products for automotive medical and aerospace applications. the following can be concluded from the results.

1. The developed regression equations demonstrated a high level of correspondence with the experimental data, indicating that the model is capable of accurately predicting the response.
2. The results of ANOVA showed that the interaction between the thickness of SS304 (mm) and voltage (V) had a significant impact on the response of the sheet metal during electromagnetic forming and GRG. However, out of all the individual parameters, voltage was found to have the greatest influence. Additionally, the factors of coil gap and SS304 thickness were also found to be significant, with contribution ratios of 7.99% and 6.07%, respectively.
3. The highest value of GRG was achieved when the electromagnetic forming settings were at their maximum levels, specifically, a SS304 sheet thickness of 0.56mm, AA6061-T6 thickness of 1.52mm, voltage of 2800V, and a coil gap of 1mm.The results indicate that there was a significant increase in elongation and die fitting responses, by 28.3% and 29% respectively. There was a slight increase in magnetic pressure of 0.6% and peak current of 0.2%.
4. The research demonstrated that by utilizing the appropriate combination of process parameters, it is possible to enhance crucial responses related to product quality, energy efficiency, and economic performance in the field of electromagnetic forming, thereby promoting sustainable manufacturing practices.

The outcome of this work can also be extended:

1. Preheated workpiece can be used instead of cold forming to analyze the deformation of SS304 alloy.
2. Other non-magnetic metals such as titanium alloys can be analyzed.

References

[1] M. Kleiner, C. Beerwald, and W. Homberg, “Analysis of process parameters and forming mechanisms within the electromagnetic forming process,” *CIRP Ann. - Manuf. Technol.*, vol. 54, no. 1, pp. 225–228, Jan. 2005, doi: 10.1016/S0007-8506(07)60089-4.

[2] V. Psyk, D. Risch, B. L. Kinsey, A. E. Tekkaya, and M. Kleiner, “Electromagnetic forming - A review,” *J. Mater. Process. Technol.*, vol. 211, no. 5, pp. 787–829, May 2011, doi: 10.1016/j.jmatprotec.2010.12.012.

[3] M. T. Nasri *et al.*, “Experimental and numerical investigation of sheet metal failure based on Johnson-Cook model and Erichsen test over a wide range of temperatures,” *Mech. Adv. Mater. Struct.*, pp. 1–14, Mar. 2022, doi: 10.1080/15376494.2022.2049934.

[4] R. Selvam and S. S. Karibeeran, “Optimisation of Process Parameters for Electromagnetic Forming of AA6101 Tubes.” Sep. 03, 2020, doi: 10.1115/MSEC2020-8354.

[5] L. Qiu *et al.*, “Analysis of Electromagnetic Force and Deformation Behavior in Electromagnetic Tube Expansion With Concave Coil Based on Finite Element Method,” *IEEE Trans. Appl. Supercond.*, vol. 28, no. 3, pp. 1–5, 2018, doi: 10.1109/TASC.2017.2789287.

[6] X. Zhang *et al.*, “Application of Triple-Coil System for Improving Deformation Depth of Tube in Electromagnetic Forming,” *IEEE Trans. Appl. Supercond.*, vol. 26, no. 4, pp. 1–4, 2016, doi: 10.1109/TASC.2016.2542482.

[7] A. G. Mamalis, D. E. Manolakos, A. G. Kladas, and A. K. Koumoutsos, "Electromagnetic forming tools and processing conditions: Numerical simulation," *Materials and Manufacturing Processes*, vol. 21, no. 4. pp. 411–423, Jul. 01, 2006, doi: 10.1080/10426910500411785.

[8] M. Soni, M. Ahmed, S. K. Panthi, and S. Kumar, "Effect of coil design parameters on performance of electromagnetic forming process," *Mater. Manuf. Process.*, vol. 37, no. 1, pp. 64–80, Jan. 2022, doi: 10.1080/10426914.2021.1945091.

[9] C.-L. Kuo, J.-S. You, and S.-F. Hwang, "Initial experiment for embossing a 3-D microstructure on the inside wall of a wound tube by an electromagnetic compression process," *J. Chinese Inst. Eng.*, vol. 34, no. 8, pp. 1025–1033, Dec. 2011, doi: 10.1080/02533839.2011.618243.

[10] J. R. Alves Z. and F. Bay, "Magnetic pulse forming: simulation and experiments for high-speed forming processes," *Adv. Mater. Process. Technol.*, vol. 1, no. 3–4, pp. 560–576, Oct. 2015, doi: 10.1080/2374068X.2015.1132723.

[11] A. Shrivastava, A. Telang, A. K. Jha, and M. Ahmed, "Experimental and numerical study on the influence of process parameters in electromagnetic compression of AA6061 tube," *Mater. Manuf. Process.*, vol. 34, no. 13, pp. 1537–1548, Oct. 2019, doi: 10.1080/10426914.2019.1655156.

[12] Z. Lai *et al.*, "Radial Lorentz force augmented deep drawing for large drawing ratio using a novel dual-coil electromagnetic forming system," *J. Mater. Process. Technol.*, vol. 222, pp. 13–20, 2015, doi: 10.1016/j.jmatprotec.2015.02.029.

[13] Q. Xiong, H. Tang, C. Deng, L. Li, and L. Qiu, "Electromagnetic Attraction-Based Bulge Forming in Small Tubes: Fundamentals and Simulations," *IEEE Trans. Appl. Supercond.*, vol. 28, no. 3, 2018, doi: 10.1109/TASC.2017.2785778.

[14] M. Seth, V. Vohnout, G. D.-J. of materials processing, and undefined 2005, "Formability of steel sheet in high velocity impact," *Elsevier*, Accessed: Oct. 31, 2020. [Online]. Available: https://www.sciencedirect.com/science/article/pii/S0924013604012129?casa_token=9cwITiaVeJUAAAAA:5fxy1mU09h2D0HfSQO3CXdcH2nyGq-AX-g7zkHHY7pDveWyk1sL8JnCjqal9o0hsFu2fXb2cFw.

[15] H. Park *et al.*, "Experimental Study on Electromagnetic Forming of High Strength Steel Sheets with Different Dimensions of Aluminum Driver Plate," no. 10040078, pp. 237–242, 2014.

[16] F. Li, J. Mo, J. Li, H. Zhou, and L. Huang, "Study on the driver plate for electromagnetic forming of titanium alloy Ti-6Al-4V," *Int. J. Adv. Manuf. Technol.*, vol. 69, no. 1–4, pp. 127–137, 2013, doi: 10.1007/s00170-013-5002-1.

[17] F. Li, J. Mo, H. Zhou, and Y. Fang, "3D Numerical simulation method of electromagnetic forming for low conductive metals with a driver," *Int. J. Adv. Manuf. Technol.*, vol. 64, no. 9–12, pp. 1575–1585, 2013, doi: 10.1007/s00170-012-4124-1.

[18] X. Deng, S. Qin, and J. Huang, "Multiobjective optimization of axially varying thickness lateral corrugated tubes for energy absorption," *Mech. Adv. Mater. Struct.*, vol. 29, no. 25, pp. 4259–4272, Oct. 2022, doi: 10.1080/15376494.2021.1924901.

[19] H. Savadkoohian, A. Fallahi Arezoodar, and B. Arezoo, "Analytical and experimental study of wrinkling in electromagnetic tube compression," *Int. J. Adv. Manuf. Technol.*, vol. 93, no. 1–4, pp. 901–914, 2017, doi: 10.1007/s00170-017-0571-z.

[20] Z. Khan, M. Khan, S. H. Imran Jaffery, M. Younas, K. S. Afaq, and M. A. Khan, "Numerical and experimental investigation of the effect of process parameters on sheet deformation during the electromagnetic forming of AA6061-T6 alloy," *Mech. Sci.*, vol. 11, no. 2, pp. 329–347, 2020, doi:

10.5194/ms-11-329-2020.

[21] D. Kumar, S. D. Kore, and A. Nandy, “Experimental investigation of Cu-SS electromagnetically assisted adhesive tube-to-tube joining: Its advantages over electromagnetic crimping,” *Int. J. Adhes. Adhes.*, vol. 109, p. 102908, 2021, doi: https://doi.org/10.1016/j.ijadhadh.2021.102908.

[22] M. Ayaz, M. Khandaei, and Y. Vahidshad, “Optimizing the mechanical properties of Al-SS joint using the numerical and experimental investigation of electromagnetic welding,” *J. Adhes. Sci. Technol.*, vol. 35, no. 20, pp. 2202–2229, Oct. 2021, doi: 10.1080/01694243.2021.1882765.

[23] M. Ayaz, M. Khandaei, and Y. Vahidshad, “Evaluating the Electromagnetic Welding Parameters for Improving the Mechanical Properties of Al–Cu Joint,” *Arab. J. Sci. Eng.*, vol. 45, no. 11, pp. 9619–9637, 2020, doi: 10.1007/s13369-020-04868-x.

[24] N. Senthilnathan, G. Venkatachalam, and N. N. Satonkar, “A Two Stage Finite Element Analysis of Electromagnetic Forming of Perforated Aluminium Sheet Metals,” *Procedia Eng.*, vol. 97, pp. 1135–1144, 2014, doi: https://doi.org/10.1016/j.proeng.2014.12.392.

[25] M. Shabanpour and A. Fallahi Arezoodar, “Multi-objective optimization of the depth of bead and tearing in electromagnetic tube compression forming,” *Int. J. Adv. Manuf. Technol.*, vol. 87, no. 1–4, pp. 867–875, 2016, doi: 10.1007/s00170-016-8519-2.

[26] “OPTIMIZATION OF PROCESS PARAMETERS IN RING.pdf.” .

[27] L. Huang, W. Feng, J. Zeng, and Z. Ding, “Research on the drive electromagnetic forming of aluminum alloy and parameter optimization,” *Int. J. Adv. Manuf. Technol.*, vol. 120, no. 11–12, pp. 7101–7113, 2022, doi: 10.1007/s00170-022-09214-z.

[28] Z. Khan *et al.*, “Dynamic Analysis of Closed Die Electromagnetic Sheet Metal Forming to Predict Deformation and Failure of AA6061-T6 Alloy Using a Fully Coupled Finite Element Model,” *Materials (Basel).*, vol. 15, no. 22, p. 7997, 2022, doi: 10.3390/ma15227997.

[29] O. Access, “Numerical and experimental investigation of fully- coupled and uncoupled finite element model for electromagnetic forming of Aluminium Alloy Al Numerical and experimental investigation of fully-coupled and uncoupled finite element model for electromagneti,” 2020, doi: 10.1088/1757-899X/999/1/012008.

[30] X. Cui, J. Li, J. Mo, J. Fang, B. Zhou, and X. Xiao, “Effect of the sheet thickness and current damping exponent on the optimum current frequency in electromagnetic forming,” *Int. J. Adv. Manuf. Technol.*, vol. 85, no. 1–4, pp. 843–851, 2016, doi: 10.1007/s00170-015-7983-4.

[31] M. Younas *et al.*, “Multi-objective optimization for sustainable turning Ti6Al4V alloy using grey relational analysis (GRA) based on analytic hierarchy process (AHP),” *Int. J. Adv. Manuf. Technol.*, vol. 105, no. 1–4, pp. 1175–1188, Nov. 2019, doi: 10.1007/s00170-019-04299-5.

[32] A. Bigdeli and M. Damghani Nouri, “Experimental and numerical analysis and multi-objective optimization of quasi-static compressive test on thin-walled cylindrical with internal networking,” *Mech. Adv. Mater. Struct.*, vol. 26, no. 19, pp. 1644–1660, Oct. 2019, doi: 10.1080/15376494.2018.1444231.

[33] P. Gao, Y. Feng, and L. Wang, “An Improved Grey Relation Analysis Method and Its Application in Dynamic Description for a Polymer Injection,” *Pet. Sci. Technol.*, vol. 32, no. 2, pp. 133–139, Jan. 2014, doi: 10.1080/10916466.2010.490806.

[34] B. O. Samuel, M. Sumaila, and B. Dan-Asabe, “Multi-objective optimization and modeling of a natural fiber hybrid reinforced composite (PxGyEz) for wind turbine blade development using

grey relational analysis and regression analysis," *Mech. Adv. Mater. Struct.*, pp. 1–19, Sep. 2022, doi: 10.1080/15376494.2022.2118404.